

Impurity bands and sequential resonant tunneling in the presence of terahertz fields

Andreas Wacker and Antti-Pekka Jauho

Mikroelektronik Centret, Danmarks Tekniske Universitet, DK-2800 Lyngby, Denmark

Stefan Zeuner and S. James Allen

Center for Terahertz Science and Technology, University of California at Santa Barbara, Santa Barbara, California 93106

(email: wacker@mic.dtu.dk)

Abstract

A theoretical and experimental study of transport in a low doped multiple quantum well structure shows that impurity bands are essential in understanding the electronic transport both with and without terahertz irradiation. A full self-contained model, which involves only the nominal parameters of the sample, agrees quantitatively with a wide range of experiments.

72.20.Ht, 73.20.Dx, 73.40.Gk

Perpendicular charge transport in biased superlattices displays a rich variety of physical phenomena: negative differential resistance [1], Bloch oscillations [2], dynamic localization [3], electric field domain formation [4], and photon-assisted transport [5,6] are but a few recently studied topics. In the case of weakly coupled multiple quantum well structures the perpendicular transport is dominated by resonant transitions between the energy levels in neighboring wells. In real systems these resonances are never sharp: they are broadened by various scattering mechanisms due to, e.g., impurities, interface roughness, phonons, or interactions between the particles themselves (see, e.g., Ref. [7]). For samples with low doping impurity scattering may lead to the appearance of impurity bands [8]. These additional narrow bands cannot be described by simple Lorentzian spectral functions thus necessitating a more detailed microscopic model. In the present paper we develop a fully microscopic model for this situation. Our calculations yield a strong temperature dependence of the current-field relation associated with the occurrence of two different peaks at low fields. The implications of these features are compared to both previously published and new experimental results.

For weakly coupled quantum wells the current from the ν^{th} level in well n to the μ^{th} level in well $n + 1$ is given by [9]

$$I_{n \rightarrow n+1}^{\nu \rightarrow \mu} = 2e \sum_{\underline{k}} |H_1^{\mu, \nu}|^2 \int_{-\infty}^{\infty} \frac{dE}{2\pi\hbar} A_{n+1}^{\mu}(\underline{k}, E + eFd) \times A_n^{\nu}(\underline{k}, E) [n_F(E - \mu_n) - n_F(E + eFd - \mu_{n+1})] . \quad (1)$$

Here e is the electron charge, μ_n is the electro-chemical potential in well n , $n_F(\mathcal{E}) = 1/[1 + \exp(\mathcal{E}/k_B T_e)]$, and T_e is the electron temperature. Fd is the voltage drop per period d . The transition matrix elements $H_1^{\mu, \nu}$ between adjacent wells are calculated using the Wannier functions obtained from a Kronig-Penney model [10]. Here we restrict ourselves to resonant transitions where the tunneling process conserves the wave vector \underline{k} within the two-dimensional electron-gas; nonresonant transitions (see Ref. [11]) are of minor significance for the sample considered here. The microscopical description of the impurity scattering enters through the spectral functions $A_n^{\nu}(\underline{k}, E)$ which are evaluated in a self-consistent single-site approximation (shown diagrammatically in the lower inset of Fig. 1) like in Ref. [8]. The homogeneous doping is modeled by 8 equally spaced δ -doping layers per period. The screening of the impurity interaction is accounted for within the random phase approximation. We restrict ourselves to the two lowest levels. For the upper level we include a contribution to the imaginary part of the self-energy due to optical phonon transitions to the ground level, calculated as in [12]. We do not consider the spin-resolved electron-electron interaction leading to the splitting of the impurity bands for a single impurity location, (the Mott transition, see e.g. [13]) because the uniform doping will lead to a smearing out of these features. The technical details of our calculation will be given elsewhere; here we point out that the theoretical framework has recently [11] been successfully applied to high-doping samples, where impurity bands play no role.

We next describe our numerical results. The upper inset of Fig. 1 shows the spectral functions for two different energies below ($E = -3$ meV) and above ($E = 2$ meV) the bottom of the (free electron) band edge. For $E = 2$ meV the spectral function exhibits a characteristic Lorentzian-type behavior with a peak around $E_k = \hbar^2 k^2 / 2m \approx 2$ meV. This is the generic behavior of a quasiparticle with a finite lifetime due to scattering. In contrast

to this behavior the spectral function is quite flat for $E = -3$ meV, which is a signature of an impurity band [8]. The density of states $\rho(E) = 2/(2\pi) \sum_{\underline{k}} A(\underline{k}, E)$ for the lowest level is plotted in Fig. 1 (full line). The impurity bands from different locations of impurities overlap and manifest themselves in a low density of states in the range $E_{\min} = -5.8$ meV $< E < 0$ below the band edge. Importantly, for these low-doped samples the Fermi level is at $E_F = -2$ meV, i.e., *within* the impurity band. As we shall see below, this property has far-reaching consequences.

We calculate the currents $I_{n \rightarrow n+1}(eFd)$ for different electron temperatures T_e by summing up the different contributions from Eq. (1). Characteristic results are shown in Fig. 2 for an electron density $6 \times 10^9/\text{cm}^2$ per well provided by the doping. Here we focus in the low field region where only tunneling between the lowest levels in each well takes place. For $T_e = 4$ K we find a maximum at $eF_{\text{high}}d \approx 5$ meV. This is due to tunneling from the impurity band to the free states. The maximum occurs at the energy where the bottom of the impurity band in one well is aligned with the band edge of the free electron states in the neighboring well, i.e., $eF_{\text{high}}d \approx |E_{\min}|$. An increasing temperature leads to a transfer of electrons from the impurity band to the free-electron states and consequently the current at $eF_{\text{high}}d$ decreases with increasing T_e . The density of states in the impurity band is much lower than in the free-electron states, and hence the majority of the electrons will be in the free-electron states for $k_B T_e \gtrsim |E_{\min}|$. For the free-electron states the overlap between the spectral functions (note that the inset of Fig. 1 is plotted in log-scale) from well n and $n+1$ is very large at small fields. This yields a strong enhancement in the low field conductivity. As the overlap of the spectral functions becomes small for voltage differences larger than their broadening, the current *decreases* for $eFd > eF_{\text{low}}d \approx 0.5$ meV. This transition from a single-peaked to a double-peaked current-field relation with increasing temperature is essential in understanding the transport in low-doped samples.

We can now resolve a recent puzzle of Ref. [14]: there it was found that peaks observed in the current-voltage characteristics (IV) under terahertz irradiation can be interpreted consistently as photon-replicas of a maximum in an “instantaneous” IV located at $U \approx 20$ mV. Yet, a direct measurement of the IV without irradiation showed no maximum at this bias. A qualitative explanation, based on impurity bands, is as follows. For low electron temperatures and without irradiation the maximum at $eF_{\text{high}}d$ dominates the domain formation which sets in at voltages exceeding $U \approx NeF_{\text{high}}d$ where $N = 10$ is the number of wells. If the THz radiation is present the electrons are excited from the impurity band into the free electron states corresponding to a larger effective electron temperature. Thus, the maximum at $U = NeF_{\text{low}}d$ is dominant, and the photon replicas corresponding to this feature are seen experimentally.

While the above consideration explains qualitatively the findings of Ref. [14], it needs to be refined to agree quantitatively with the experiment: the experimental photon-replica suggest $eF_{\text{low}}^{\text{exp}}d \approx 2$ meV which is four times the value from Fig. 2. The domain formation sets in at $U = 0.1$ V yielding $eF_{\text{high}}^{\text{exp}}d \approx 10$ meV (i.e., twice larger than $eF_{\text{high}}d$ of Fig. 2), which seems to require $|E_{\min}| \sim 10$ meV. This value follows from our theory as well, as we now argue. The screening of the impurity potential was treated using a free electron density-of-states $\rho_0 = m/\pi\hbar^2$ yielding the polarizability $\Pi(k) = \rho_0 [1 - \theta(k - 2k_F)\sqrt{1 - 4(k_F/k)^2}]$. Now $\Pi(0)$ is related to the *actual density of states* at $E_F \approx -2$ meV which is significantly lower than ρ_0 . Calculations within the Born-approximation show that the k -dependence of

the polarizability becomes weaker and that $\Pi(0)$ decreases with increasing scattering [15,16]. In order to accommodate these trends we make the replacement $\Pi(k) \rightarrow \Pi^*(k) = 0.07\rho_0$, given by the calculated density of states of Fig. 1, and use this value in further calculations. The smaller polarizability weakens the screening of the impurity potential and therefore increases the binding energy of the impurities [8]. The resulting density of states is shown in Fig. 1 by a dashed line. The onset of the impurity band is now $E_{\min} = -9.1$ meV and the current-field characteristics look similar to Fig. 2 but with $eF_{\text{low}}d = 2$ meV, $eF_{\text{high}}d = 8.2$ meV in good agreement with the values deduced from the experiment.

As a further test of the theory, we next consider the temperature dependence of the zero-bias conductance σ . Eq. (1) yields $\sigma(T) \propto \int dE \sum_{\underline{k}} A(\underline{k}, E)^2 \partial n_F(E) / \partial E$, which implies $\sigma(T) \propto 1/T$ for $k_B T \gg E_F - E_{\min}$ and $\sigma(T) \rightarrow \text{const.}$ for $k_B T \ll E_F - E_{\min}$, provided that $\sum_{\underline{k}} A(\underline{k}, E)^2$ has no strong energy dependence. This is the case if impurity scattering is treated within the self-consistent Born approximation where no impurity bands form. Then σ is monotonously decreasing in T as shown in Fig. 3. However, a different scenario emerges if the electrons occupy impurity bands for low temperatures. Then σ is strongly suppressed due to the small values of $A(\underline{k}, E)$ for $E < 0$, see Fig. 1. As temperature is increased, more electrons are excited to the free electron states, and σ *increases* with T until the impurity bands are almost empty at $k_B T \sim |E_{\min}|$. This physical picture is confirmed by our measurements, shown in Fig. 3, together with our full calculation. At low temperatures the agreement is quantitative, while at intermediate T the theory overestimates σ ; this is most likely due to additional scattering processes not included in our calculation, or by the presence of a contact resistance which may limit the experimental conductance.

In order to calculate the full current-voltage characteristic we must consider electron heating, i.e., estimate the parameter T_e in Eq. (1). With average voltage drop of 8 mV per well we find experimentally $I = 0.57 \mu\text{A}$ without irradiation. This gives a power dissipation of $P = 9$ pW per electron and a temperature of $T_e \approx 47$ K using the standard energy loss by optical phonons [17], $\hbar\omega_{\text{LO}}/\tau_{\text{LO}} \exp(-\hbar\omega_{\text{LO}}/kT_e)$ with $\tau_{\text{LO}} \approx 80$ fs. An increase of the energy loss with decreasing electron density has been predicted due to plasmon-phonon coupling [17]. Recently, $P = 9$ pW at $T_e \approx 40$ K for a sample with an electron density $6 \times 10^{10}/\text{cm}^2$ per period has been reported [18]. As our density is much smaller an even lower electron temperature is possible. Experimentally, we find that the current-voltage characteristics exhibits a plateau for $0.04 \text{ V} < U < 0.1 \text{ V}$ with $I = 0.57 \mu\text{A}$ (see Fig. 4). The current of this plateau remains almost constant for lattice temperatures between 2 K and 30 K, but drops for higher temperatures. This can be understood if the electron heating prevents the electron temperature from cooling below 30 K. All these facts indicate that $T_e \approx 30$ K is a consistent choice for medium voltages. For vanishing bias, on the other hand, the electron temperature must approach the lattice temperature (4K).

The IV including domain formation [19] is calculated as in Ref. [11] and is shown in Fig. 4. We find excellent agreement with the data for the maximum current for the first peak ($I_{1,\text{th}}^{\text{peak}} = 0.8 \mu\text{A}$; $I_{1,\text{exp}}^{\text{peak}} = 0.58 \mu\text{A}$) and the second peak at higher voltages ($I_{2,\text{th}}^{\text{peak}} = 11 \mu\text{A}$; $I_{2,\text{exp}}^{\text{peak}} = 13.6 \mu\text{A}$, not shown in the figure). The voltage where domain formation sets in is in good agreement with the experimental value, but the domain branches occur at higher voltages in the experiment. This can be explained by the fact that once the high field domain is formed it extends into the low doped receiving contact region where a voltage drop of 0.1 V may occur.

Finally, we consider the sample in a strong terahertz field from a free-electron laser with frequency ν and field strength F_{ac} . Following Refs. [5,14,20] we use the relation

$$I_{n \rightarrow n+1}^{\text{irr}} = \sum_{l=-\infty}^{\infty} [J_l(\alpha)]^2 I_{n \rightarrow n+1}(eF_{ac}d + lh\nu), \quad (2)$$

where $\alpha = eF_{ac}d/(h\nu)$ and J_l is the ordinary Bessel function of order l . This formula was originally derived for tunneling through a single barrier [21] and holds within a miniband model for superlattices as well [22]. However, modifications due to photon side-bands from a single quantum well [23] have been suggested. According to the arguments presented above, we model the nonequilibrium distribution function by assuming an electron temperature of 35 K. Then only 48 % of the electrons are occupying the states below $E = 0$. Quantitative agreement between theory (Fig. 5a) and experiment (Fig. 5b) is found for $h\nu = 6.3$ meV (1.5 THz) for different strengths of the laser field [24]. We find a direct tunneling peak at $U_{\text{dir}} = NF_{\text{low}}d \approx 20$ mV and photon replicas at $U \approx U_{\text{dir}} + Nh\nu/e$ and $U \approx U_{\text{dir}} + 2Nh\nu/e$. For low bias and high intensities there is a region of absolute negative conductance (NC) [6] which is studied for different frequencies in the following. In the experiment at each frequency the laser power was chosen to give maximum NC near zero bias. As can be seen from Fig. 5(d) a minimum in current occurs at $U \approx -U_{\text{dir}} + Nh\nu/e$. This is just the photon replica of the direct tunneling peak on the negative bias side [14] which dominates if the direct tunneling channel is suppressed close to the zero of $J_0(\alpha)$ in Eq. (2), i.e., $\alpha \approx 2.4$, as used in the calculation (Fig. 5c). For $h\nu = 5.3$ meV a smaller value of α (thin line) agrees better with the experimental data. This may be related to charge accumulation effects inside the sample weakening the NC, so that maximum NC is observed at a laser field corresponding to a lower value of α . Both the theoretical and experimental result show that absolute NC is persistent in a wide range of frequencies but becomes less pronounced with decreasing photon energy.

In conclusion, we have presented a self-contained theory of transport in low doped and weakly coupled quantum wells. A detailed comparison with several different experiments shows that: (i) it is necessary to consider impurity bands; (ii) excellent agreement between theory and experiment is achieved for static and irradiated IV as well as zero-bias conductance using reduced screening, and (iii) the simple relation (2) provides a quantitative description of photon-assisted transport in multiple quantum wells.

We want to thank Ben Hu for stimulating discussions. A.W. and S.Z. acknowledge financial support by the Deutsche Forschungsgemeinschaft. Work performed at the Center for Terahertz Science and Technology was supported by the Office of Naval Research, the Army Research Office and the National Science Foundation.

REFERENCES

- [1] L. Esaki and R. Tsu, IBM J. Res. Develop. **14**, 61 (1970).
- [2] C. Waschke *et al.*, Phys. Rev. Lett. **70**, 3319 (1993).
- [3] D. H. Dunlap and V. M. Kenkre, Phys. Rev. B **34**, 3625 (1986); M. Holthaus, Phys. Rev. Lett. **69**, 351 (1992).
- [4] H. T. Grahn, R. J. Haug, W. Müller, and K. Ploog, Phys. Rev. Lett. **67**, 1618 (1991); F. Prengel, A. Wacker, and E. Schöll, Phys. Rev. B **50**, 1705 (1994); L. L. Bonilla *et al.*, Phys. Rev. B **50**, 8644 (1994).
- [5] B. J. Keay *et al.*, Phys. Rev. Lett. **75**, 4098 (1995).
- [6] B. J. Keay *et al.*, Phys. Rev. Lett. **75**, 4102 (1995).
- [7] S. Q. Murphy, J. P. Eisenstein, L. N. Pfeiffer, and K. W. West, Phys. Rev. B **52**, 14825 (1995).
- [8] A. Gold, J. Serre, and A. Ghazali, Phys. Rev. B **37**, 4589 (1988); *ibid* **39**, 8499 (1989).
- [9] G. D. Mahan, *Many-Particle Physics* (Plenum, New York, 1990).
- [10] The sample [6,14] consists of 10 wells (15 nm GaAs) and 11 barriers (5 nm Al_{0.3}Ga_{0.7}As) with area $8\mu\text{m}^2$ and is homogeneously doped by $3 \times 10^{15}/\text{cm}^3$. We use the band structure parameters: $\Delta E_c = 0.24$ eV, $m_{\text{well}} = 0.067m_e$ $m_{\text{barrier}} = 0.0931m_e$ from *Properties of Aluminium Gallium Arsenide*, edited by S. Adachi (INSPEC, London, 1993).
- [11] A. Wacker and A.-P. Jauho, Superlattices and Microstructures, in print (cond-mat/9610119).
- [12] R. Ferreira and G. Bastard, Phys. Rev. B **40**, 1074 (1989).
- [13] B. I. Shklovskii and A. L. Efros, *Electronic Properties of Doped Semiconductors* (Springer, Berlin, 1984).
- [14] S. Zeuner *et al.*, Phys. Rev. B **53**, 1717 (1996).
- [15] T. Ando, J. Phys. Soc. Jpn. **51**, 3215 (1982).
- [16] S. Das Sarma, Phys. Rev. Lett. **50**, 211 (1983).
- [17] S. Das Sarma, in *Hot Carriers in Semiconductor Nanostructures*, edited by J. Shah (Academic Press, Boston, 1992).
- [18] W. Hilber, M. Helm, K. Alavi, and R. N. Pathak, Appl. Phys. Lett. **69**, (1996), in print.
- [19] We use $T_e = 4K + 26K\sqrt{eFd/8\text{meV}}$ for $eFd < 8$ meV and $T_e = 30K$ for $eFd > 8$ meV. The boundary conditions are $n_0 = 1.1N_D$, $n_{11} = N_D$ to model the charge accumulation at the injecting contact.
- [20] G. Platero, R. Aguado, and J. Iñarrea, in *Proc. 23rd Int. Conf. Phys. Semicond., Berlin 1996*, edited by M. Scheffler and R. Zimmermann (World Scientific, Singapore, 1996), p. 2263.
- [21] J. R. Tucker and M. J. Feldman, Rev. Mod. Phys. **57**, 1055 (1985).
- [22] A. A. Ignatov *et al.*, Z. Phys. B **98**, 187 (1995).
- [23] M. Wagner, Phys. Rev. Lett. **76**, 4010 (1996).
- [24] Note that the calculated currents are slightly too large for the unirradiated case and slightly too small with irradiation. This discrepancy may be related to deviations from the effective temperature model used for the electron distribution functions.

FIGURES

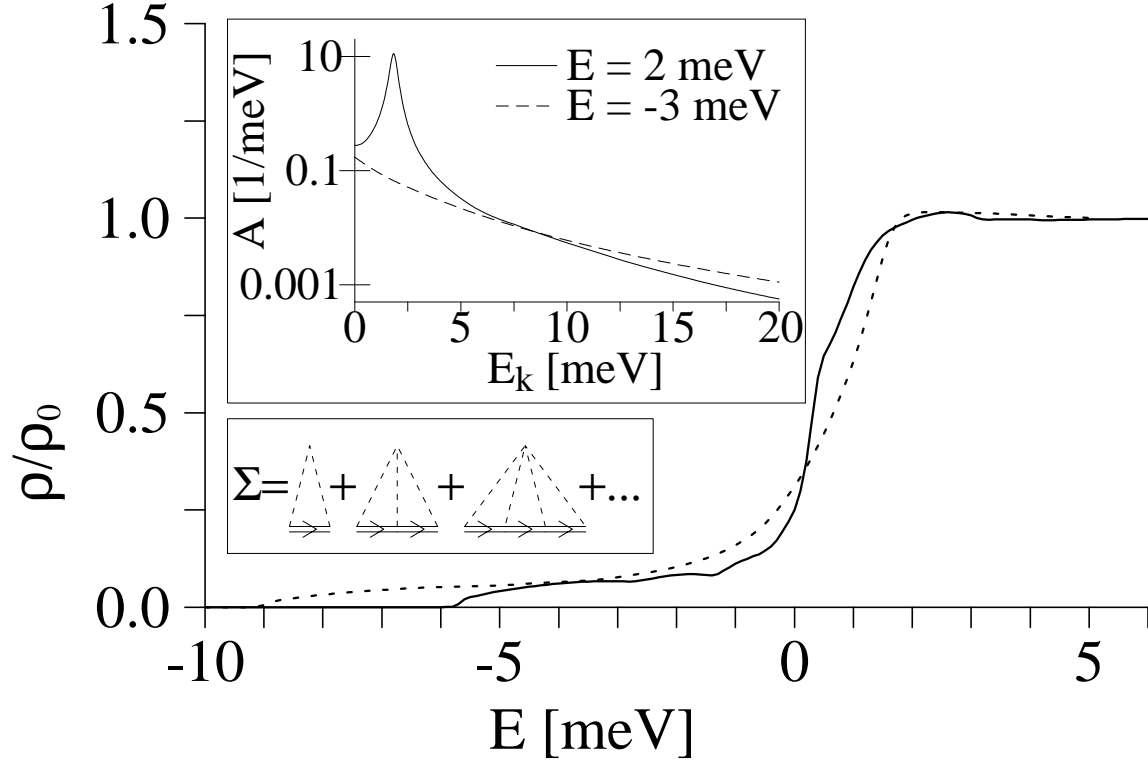


FIG. 1. Calculated density of states in units of the 2D free carrier density ρ_0 using screening due to a free electron gas (full line) and reduced screening (dashed line). The upper inset shows the spectral function $A(E_k, E)$ for different energies E . The lower inset depicts diagrammatically the self-consistent single-site approximation.

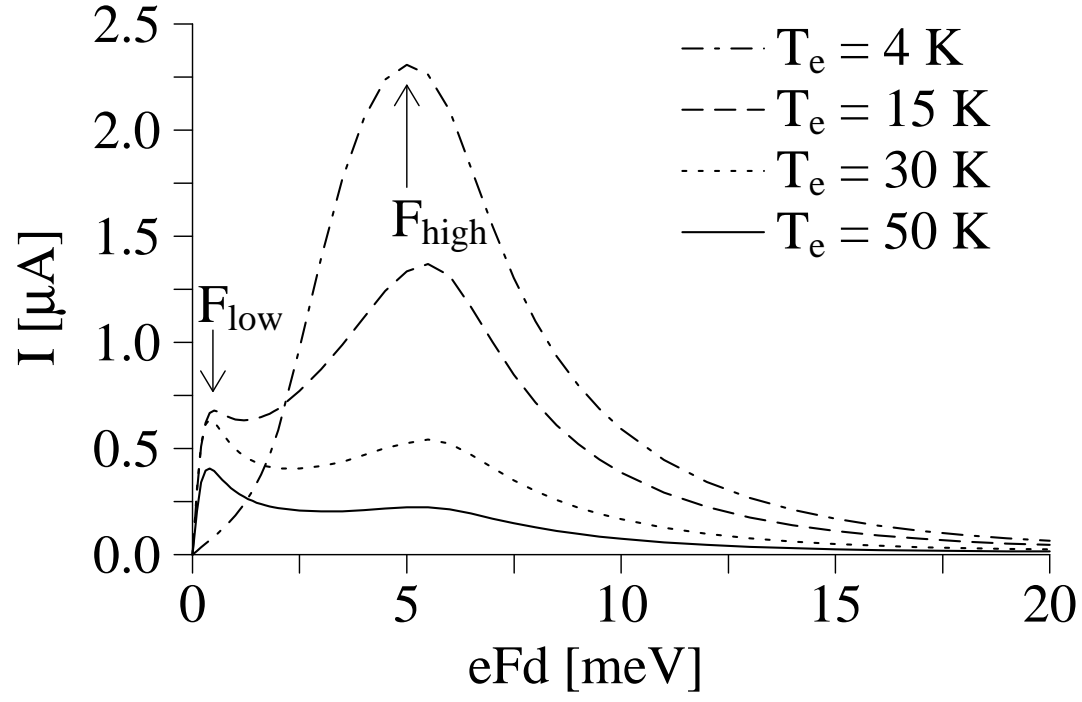


FIG. 2. Current-field relation for different electron temperatures.

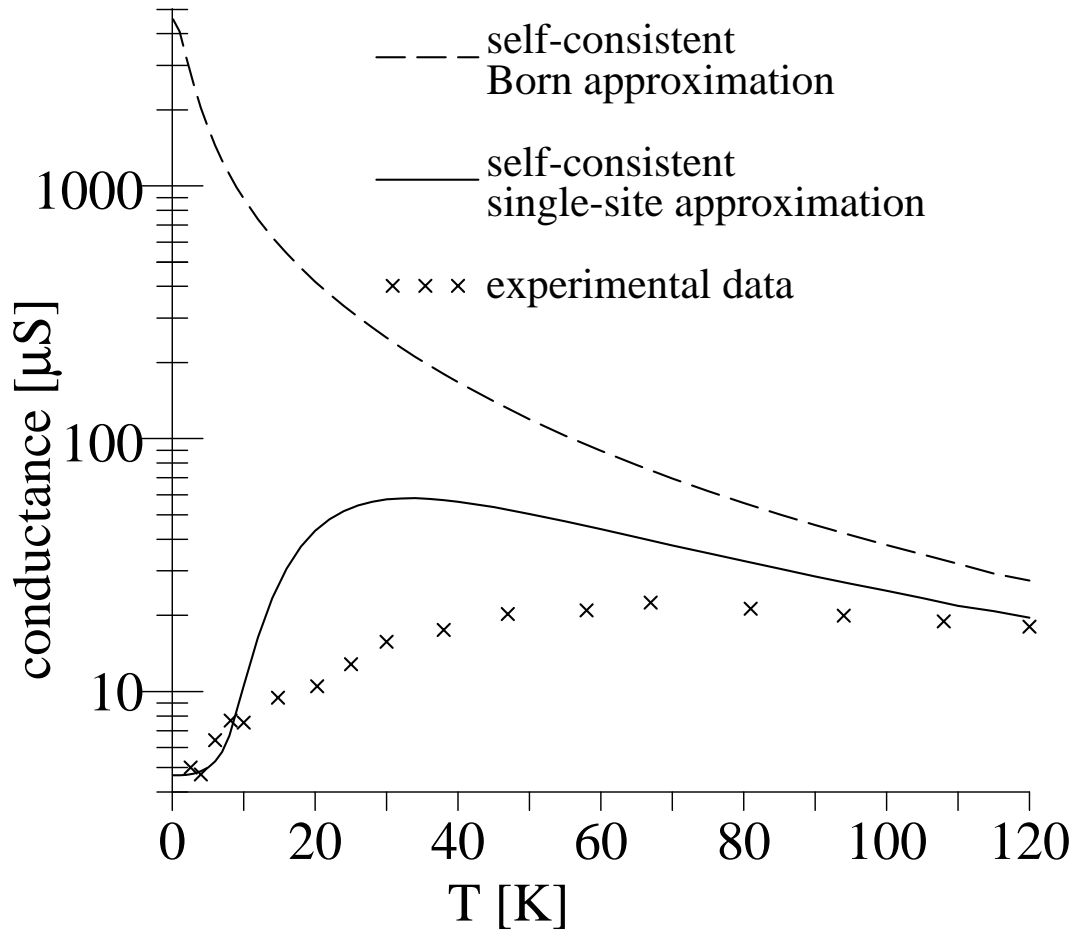


FIG. 3. Comparison of experimental and theoretical conductance at zero bias versus temperature.

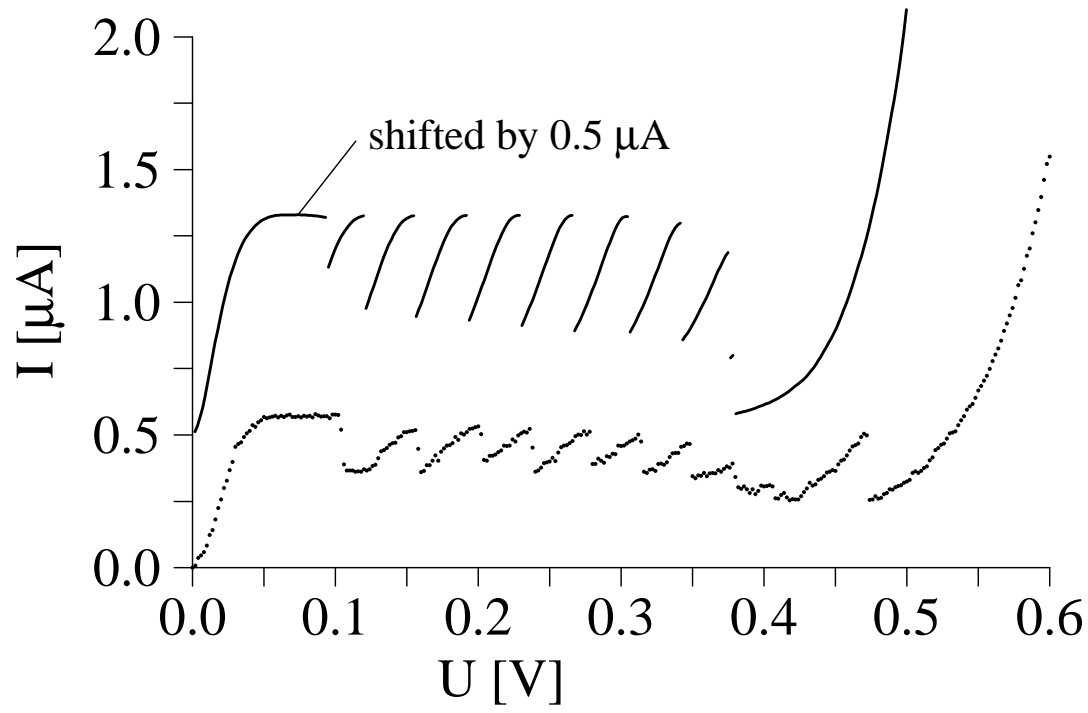


FIG. 4. Experimental (dots) and theoretical (full line) current-voltage characteristics without irradiation.

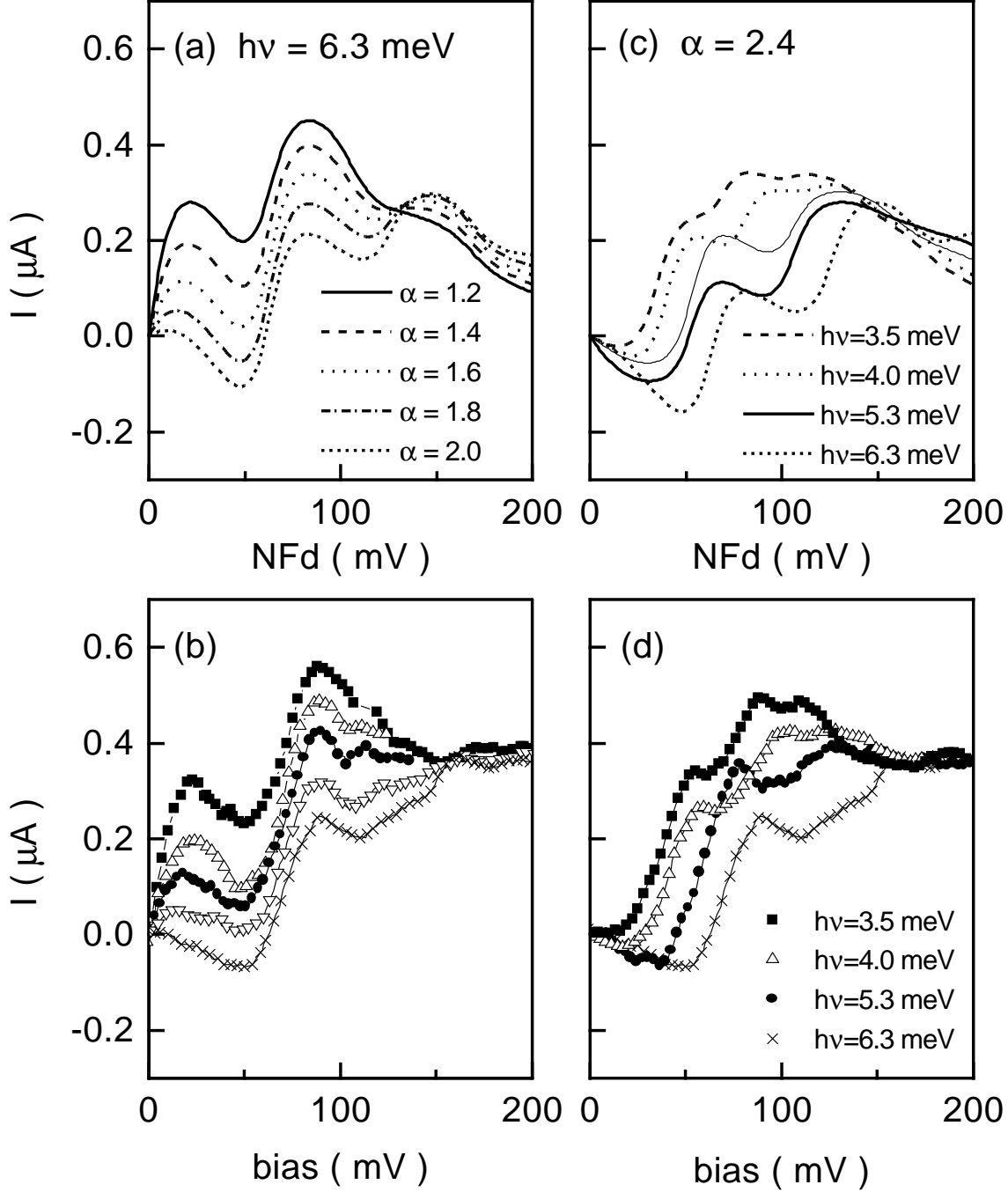


FIG. 5. Current-voltage characteristics under irradiation. a) Theoretical results for $h\nu = 6.3$ meV and different field strength $eF_{ac}d = \alpha h\nu$ of the irradiation. b) Experimental results for $h\nu = 6.3$ meV and different laser intensities increasing from the top to the bottom. The actual values F_{ac} inside the sample are not accessible. c) Theoretical results for $\alpha = 2.4$ and different photon energies. The thin line depicts $h\nu = 5.3$ meV and $\alpha = 2.1$. d) Experimental results for different photon energies. The laser intensity was chosen to give maximum negative conductance.